2-23-2007

Structure/function analysis of the interaction of phosphatidylinositol 4,5-bisphosphate with actin-capping protein: Implications for how capping protein binds the actin filament

Kyoungtae Kim

Michelle E. McCully

Nandini Bhattacharya

Boyd Butler

David Sept

See next page for additional authors

Recommended Citation

Kim, Kyoungtae, Michelle E. McCully, Nandini Bhattacharya, Boyd Butler, David Sept, and John A. Cooper. "Structure/function analysis of the interaction of phosphatidylinositol 4, 5-bisphosphate with actin-capping protein: implications for how capping protein binds the actin filament." Journal of Biological Chemistry 282, no. 8 (2007): 5871-5879.

THE JOURNAL OF BIOLOGICAL CHEMISTRY VOL. 282, NO. 8, pp. 5871–5879, February 23, 2007

Structure/Function Analysis of the Interaction of Phosphatidylinositol 4,5-Bisphosphate with Actin-capping Protein

*IMPLICATIONS FOR HOW CAPPING PROTEIN BINDS THE ACTIN FILAMENT**[S]

Received for publication, October 19, 2006, and in revised form, December 1, 2006 Published, JBC Papers in Press, December 19, 2006, DOI 10.1074/jbc.M609850200

Kyoungtae Kim[‡1], **Michelle E. McCully**[§1,2], **Nandini Bhattacharya**[‡3], **Boyd Butler**[‡], **David Sept**[§], **and John A. Cooper**[‡4]

From the [‡]*Department of Cell Biology and Physiology and the* [§]*Department of Biomedical Engineering and Center for Computational Biology, Washington University, St. Louis, Missouri 63110*

The heterodimeric actin-capping protein (CP) can be inhibited by polyphosphoinositides, which may be important for actin polymerization at membranes in cells. Here, we have identified a conserved set of basic residues on the surface of CP that are important for the interaction with phosphatidylinositol 4,5-bisphosphate (PIP_2). Computational docking studies predicted the identity of residues involved in this interaction, and functional and physical assays with site-directed mutants of CP confirmed the prediction. The PIP_2 binding site overlaps with the more important of the two known actin-binding sites of CP. Correspondingly, we observed that loss of PIP_2 binding correlated with loss of actin binding among the mutants. Using TIRF (total internal reflection fluorescence) microscopy, we observed that PIP_2 rapidly converted capped actin filaments to a growing state, consistent with uncapping. Together, these results extend our understanding of how CP binds to the barbed end of the actin filament, and they support the idea that CP can "wobble" when bound to the barbed end solely by the C-terminal "tentacle" of its β-subunit.

Actin polymerization is essential for many biological phenomena, including the cell migration that occurs as part of chemotaxis, development, and cancer. Cells regulate the location and timing of actin polymerization with remarkable precision. In cells, actin filaments grow primarily by the addition of subunits to free, barbed ends of filaments. Free barbed ends can be created by actin nucleation factors, such as Arp2/3 complex and formins, and by actin-severing proteins, such as ADF/cofilin and gelsolin. Capping proteins bind to free barbed ends and thereby halt the polymerization process.

The α/β heterodimeric capping protein, referred to here as CP,[5] is a capper found in essentially every eukaryotic organism and in every vertebrate cell and tissue type (reviewed in Ref. 1). In vertebrate striated muscle, a sarcomere-specific isoform of CP at the Z-line caps the barbed ends of the actin-based thin filaments, leading to the name CapZ. Cells lacking CP show a range of morphologic and developmental defects, based on improper actin assembly and cell motility. In *Drosophila*, loss of CP is lethal during embryogenesis.

Typical vertebrate cultured cells contain lamellipodial and filopodial processes on their surface, which are based on actin filaments organized into branched networks and straight bundles, respectively. In each case, barbed ends are oriented predominantly toward the plasma membrane, and the local capping of barbed ends is crucial. The branched networks of filaments in lamellipodia are nucleated from Arp2/3 complex, as described in the dendritic nucleation model (2). Capping of the barbed ends over time is a necessary feature of this model in order to keep the filaments short, which makes the branched network stiff, and to restrict or "funnel" polymerization to the newly created barbed ends near the membrane. Inhibition of CP essentially abolishes the formation of lamellipodia and branched networks (3). In such cells, filopodia formation is greatly enhanced, which contributes to the notion that localized inhibition of CP at one place on the membrane may be essential for a filopodium to form.

In vitro, actin-based motility can be reconstituted from pure proteins with a mixture of Arp2/3 complex, ADF/cofilin, and CP (4). Here, the dependence of motility on CP concentration was a bell-shaped curve, suggesting that optimal levels of capping may be crucial for actin-based motility in cells. Indeed, Arp2/3-mediated actin assembly as part of endocytosis in yeast does depend on optimal CP activity (5).

CP is active in the absence of calcium and under a wide range of buffer conditions. However, cells contain a number of proteins that are able to bind to and inhibit CP, such as V-1/myotrophin, CKIP-1, CD2AP, and CARMIL (6–9). In addition, polyphosphoinositides such as phosphatidylinositol 4,5-

* This work was supported in part by National Institutes of Health Grants GM38542 (to J. A. C.) and GM067246 (to D. S.). The costs of publication of this article were defrayed in part by the payment of page charges. This article must therefore be hereby marked "*advertisement*" in accordance with 18 U.S.C. Section 1734 solely to indicate this fact.

[S] The on-line version of this article (available at http://www.jbc.org) contains supplemental Tables I and II, Fig. 1, and Movie 1.

[1] These authors made equal contributions to this work.

[2] Supported in part by a Washington University/Howard Hughes Medical Inst. summer undergraduate research fellowship funded by an Undergraduate Biological Sciences Education Program Grant from the Howard Hughes Medical Institute to Washington University.

[3] Supported by National Institutes of Health Institutional Training Grant T32 HL007873.

[4] To whom correspondence should be addressed: Campus Box 8228, 660 S. Euclid Ave., St. Louis, MO 63110. Tel.: 314-362-3964; Fax: 314-362-7463; E-mail: jcooper@wustl.edu.

[5] The abbreviations used are: CP, capping protein; PIP_2, phosphatidylinositol 4,5-bisphosphate; TIRF, total internal reflection fluorescence; DTT, dithiothreitol.

bisphosphate (PIP_2) can bind and inhibit CP (10). Of note, PIP_2 appears to be able to remove CP from capped barbed ends (11), which may help to stimulate actin assembly in certain situations in cells. During platelet activation, an initial step appears to be release of CP from the actin cytoskeleton by PIP_2 (12); later in the process, CP appears to return to the actin cytoskeleton, presumably binding newly formed barbed ends. Association of CP with the actin cytoskeleton is also seen with actin assembly in *Dictyostelium* cells responding to chemoattractant (13).

The crystal structure of CP shows the α- and β-subunits arranged with a pseudo-2-fold rotational axis of symmetry (14). In molecular dynamics simulations, the C-terminal region of the β-subunit is highly mobile, and the C-terminal region of the α-subunit remains closely apposed to the surface of the protein (6), as suggested by the crystal structure. A recent cryo-electron microscopy analysis of CP bound to the barbed end of the actin filament shows the top surface of CP in contact with actin, with the C-terminal regions of each subunit as likely sites of close contact (15). In biochemical studies, the C-terminal region of each subunit appears to be able to bind to the barbed end, and those interactions are independent of each other (16, 17). When both actin-binding sites are intact, CP binds to the barbed end with subnanomolar affinity because of a low off-rate constant (17).

Our current view of the interaction of CP with the filament barbed end includes the hypothesis that when CP is attached solely by its β-tentacle, it is able to wobble. This exposes the top surface of the protein, which includes the actin-binding site near the α-subunit C terminus. Recent findings with the protein V-1/myotrophin support this view (6). V-1 appears to bind the β-subunit C terminus, and V-1 inhibits capping but does not uncap, as predicted by the hypothesis. Another prediction of the hypothesis is that a molecule that is able to uncap should bind to the top surface of the protein, and this interaction should be independent of the β-tentacle.

In this study, to gain insight into how PIP_2 binds CP, how PIP_2 binding inhibits CP, and how CP binds actin, we wanted to perform a structure/function analysis with site-directed mutagenesis to identify regions of CP necessary for interaction with PIP_2. We also performed computational modeling of CP/PIP_2 interactions to help guide the mutagenesis and to provide independent and complementary evidence regarding the nature of the interaction. In addition, we sought new evidence for the uncapping effect of PIP_2, with direct visualization of actin filament growth in real time by TIRF microscopy. Finally, we wanted to use these results to test the wobble model for the interaction of CP with the filament barbed end.

EXPERIMENTAL PROCEDURES

Chemicals and reagents were from Fisher Scientific and Sigma unless stated otherwise. PIP_2 and 1,2-di-oleyoyl ethylene glycol (diacylglycerol) were obtained from Avanti (Alabaster, AL). Synthetic acyl-chain variants of PIP_2 with diC_4, diC_8, and diC_{16} were obtained from Echelon Biosciences (Salt Lake City, UT). Concentrated phospholipid stock solutions were prepared and handled as described (28).

Plasmid Construction and Mutagenesis—Site-directed mutations were created in a chicken CP $\alpha1\beta1$ pET bacterial expression plasmid (pBJ994) (18) by PCR using the QuikChange method (Stratagene, La Jolla, CA). Primers and plasmids are listed in supplemental Tables I and II, respectively. pET-3d/CPα(K256A)β, encoding a K256A mutation in the α-subunit, was constructed using forward primer KKT 255 and reverse primer KKT 256. pET-3d/CPα(R260A)β, encoding an R260A mutation in the α-subunit, was constructed using KKT 216 and 217. pET-3d/CP$\alpha\beta$(K95A), encoding a K95A mutation in the β-subunit, was constructed using KKT 205 and KKT 206. pET-3d/CPα(KR256,260AA)β, encoding a R256A,K260A mutation in the α-chain, was constructed using pET-3d/CPα(K256A)β as template and primers KKT 216 and KKT 217. pET3d/CPα(RK266, 268AA)β, encoding an RK266, 268AA mutation in the α-subunit, was constructed using KKT 214 and KKT 215. pET-3d/CPα(R256A,K260A)β(R225A), encoding a R256A,K260A mutation in the α-subunit and an R225A mutation in the β-subunit, was constructed with primers KKT 257 and KKT 258 using pET-3d/CPα(R256A,K260A)β as a template plasmid.

Proteins—CP was expressed in bacteria and purified as described (16) with minor modifications for mutants. Purified proteins were stored at −20 °C in 10 mM Tris-HCl, pH 7.5, 50 mM KCl, 1 mM $MgCl_2$, 1 mM EGTA, 0.5 mM DTT, and 50% glycerol. Muscle actin was purified and labeled with pyrene as described (17). Spectrin-F-actin seeds were prepared from human erythrocytes as described (19). Actin capping assays were performed as described (16).

Rabbit skeletal muscle myosin (Cytoskeleton, Inc., Denver, CO) (10 μM) was dialyzed against 10 mM imidazole, pH 7, 0.5 M KCl, 10 mM EDTA for 2 h. Following a 1-h incubation with 1 mM *N*-ethylmaleimide on ice, 1 mM DTT was added for 1 h on ice. *N*-ethylmaleimide-myosin was dialyzed overnight against 50% glycerol in 10 mM imidazole, pH 7, 0.5 M KCl, 10 mM EDTA, 1 mM DTT and stored at −20 °C.

Fitting of Actin Polymerization Reactions—Binding constants for CP with actin and lipids were determined by least-squares fitting of full time course data using Berkeley Madonna 8.3 as described (17) with the following kinetic mechanism. In these reactions, A is actin monomer, N_b is free barbed end, CP is capping protein, and L is lipid. In this simple scheme, the capped barbed end, CPN_b, can neither add nor lose actin subunits; the complex of CP with lipid, CPL, cannot interact with a barbed end.

$$A + N_b \underset{k_-}{\overset{k_+}{\rightleftharpoons}} AN_b$$

REACTION 1

$$AN_b + CP \underset{k_{-cap}}{\overset{k_{+cap}}{\rightleftharpoons}} CPN_b$$

REACTION 2

$$CP + L \underset{k_-}{\overset{k_+}{\rightleftharpoons}} CPL$$

REACTION 3

For Reaction 1, k_+ was 11.6 μM^{-1} s^{-1} and k_- was 1.4 s^{-1} (20). The rate constants for capping in Reaction 2 were determined by fitting the experimental data for seeded actin assembly in the presence of CP. A range of CP concentrations was used, generating a family of curves, and they were fit together. The rate constants for CP binding to lipid in Reaction 3 were determined by fitting a set of curves produced by addition of PIP_2 at various concentrations.

Tryptophan Quenching Assay for CP/Lipid Interaction—The equilibrium dissociation constant, K_d, for the binding of CP to phospholipid was determined by measuring the quenching of intrinsic tryptophan fluorescence as described (21) with minor modifications. Briefly, fluorescence emission spectra (300–400 nm) were collected using a PTI Quantmaster spectrofluorometer (Photon Technology International, Birmingham, NJ) with excitation at 292 nm. The mixture of CP and phospholipid was incubated for 5 min before was fluorescence measured. The maximum fluorescence intensity (ΔF) was plotted against the total concentration of PIP_2, and K_d was determined by least-squares fitting as described (21).

TIRF Microscopy—To image the polymerization of individual actin filaments, we used TIRF microscopy essentially as described (22). The system included an inverted microscope (IX-81, Olympus America, Center Valley, PA), an electron-multiplication back-thinned frame transfer charge-coupled device video camera (Model C9100-12, Hamamatsu Photonics, Bridgewater, NJ) with a 60× 1.45 numerical aperture PlanApo oil objective. SlideBook software (Intelligent Imaging Innovations, Denver, CO) operated the system and collected the images. Frames of 1500-ms duration were collected every 2–3 min. Measurements of filament length *versus* time were obtained.

To construct the microscope flow chamber, No. 0 sapphire coverslips were sonicated in a water bath sonicator for 45 min in 2% (v/v) VersaClean detergent in hot tap water, rinsed in hot tap water, and sonicated for 30 min in hot tap water. Coverslips were rinsed in distilled water, incubated for 3 h in 1 M KOH at 42 °C, rinsed in deionized distilled water, and incubated overnight in 1 M HCl at 42 °C. They were cooled to room temperature, rinsed in deionized distilled water, sonicated for 30 min in deionized distilled water, rinsed twice in 5 mM EDTA, and sonicated for 30 min in EDTA. They were rinsed in 70% ethanol, sonicated for 30 min in 70% ethanol, rinsed in absolute ethanol, sonicated for 30 min in absolute ethanol, and rinsed and stored in absolute ethanol.

Flow cell chambers were prepared as described (23). A clean sapphire coverslip was removed from ethanol and dried. Parafilm strips were stretched to approximately three times their length and placed across the long axis of the coverslip. A conventional glass slide was placed on and perpendicular to the parafilm strips. Pressure was applied and the chamber was flamed briefly to seal it. Solutions were flowed into the chamber via capillary action.

For actin polymerization experiments, unlabeled and Alexa Fluor 488-labeled rabbit muscle actin (Invitrogen) were dialyzed overnight against G buffer and then centrifuged at 100,000 × *g* for 2 h. The upper two-thirds of the supernatant was taken, and the actin concentration was measured by absorbance at 290 nm. Ca-ATP-actin was converted to Mg-ATP-actin by incubation with a 1/10 volume of 10 mM EGTA/0.2 mM $MgCl_2$ at 23 °C for 2 min. *N*-ethylmaleimide-inactivated myosin at 0.1 μM in high salt Tris-buffered saline (HS-TBS; 50 mM Tris-Cl, pH 7.6, 600 mM NaCl) was flowed into the chamber and incubated for 1 min at room temperature. The chamber was washed with 1% bovine serum albumin in HS-TBS followed by 1% bovine serum albumin in low salt Tris-buffered saline (50 mM Tris-HCl, pH 7.6, 50 mM NaCl).

To polymerize actin filaments, Mg-ATP-actin with 10% Alexa-labeled actin was mixed 1:1 with 2× polymerization buffer (100 mM KCl, 0.2 mM $MgCl_2$, 2 mM EGTA, 20 mM imidazole, pH 7.0, 100 mM DTT, 0.4 mM ATP, 30 mM glucose, 2% methylcellulose, 40 μg/ml catalase, 200 μg/ml glucose oxidase) giving a final actin concentration of 2 μM. 0.25 nM spectrin-F actin seeds were added immediately. After 10 min at room temperature, 10 nM CP $\alpha1\beta1$ was added. After another 10 min, 10 μl of this mixture was loaded into the flow chamber. The actin filaments were monitored for several min to document the absence of growth, and then various concentrations of PIP_2 were added along with 2 μM Mg-ATP actin (30% labeled) in polymerization buffer. Actin filament growth was monitored. The rate of filament growth was measured, as was the percentage of filaments growing over time. The rate of incorporation was converted to subunits/s assuming 370 subunits/μm (24).

Molecular Simulations—The starting point for our computational work was a molecular dynamics simulation of CP (Protein Data Bank code 1IZN) performed using NAMD (25). We used the CHARMM27 force field, TIP3P waters, particle mesh Ewald, Berendsen temperature, and pressure coupling (NPT ensemble) and 2-fs time steps. The heating was performed in 50,000 steps with α-carbon constraints, equilibrated at 300,000 without constraints, followed by a 5-ns production trajectory. Five representative structures of CP were extracted from the simulation at 800-ps intervals. Because the macromolecule is held rigid in molecular docking simulations, using multiple protein snapshots allowed us to capture some degree of side chain and backbone flexibility, resulting in significantly improved docking results (26). The molecular docking was carried out using AutoDock 3.0 (27). As PIP_2 is somewhat cumbersome to deal with as a full molecule, we used a modified form where the alkyl tails were truncated, leaving just the inositol and diacylglycerol groups (supplemental Fig. 1). This truncated version of PIP_2 was minimized using the Tripos force field, and Gasteiger-Marsili charges were assigned, all using Sybyl 6.8 (Tripos Inc., St. Louis, MO). Docking was performed using the Lamarckian genetic algorithm in AutoDock. Initial docking runs using the entire CP structure showed a preference for the region around the base of the α-tentacle. Based on these results, we constructed 0.2-Å spaced grids centered on the α-tentacle. 20 docking runs were completed for each of the five CP structures resulting in a total of 100 predictions. These results were clustered with a 3-Å cutoff, resulting in single, top-predicted structure that was used in subsequent analysis.

RESULTS

Structural Features of PIP_2 Important for Interaction with CP—We asked what features of PIP_2 were important for its interaction with CP. To measure these interactions, we tested

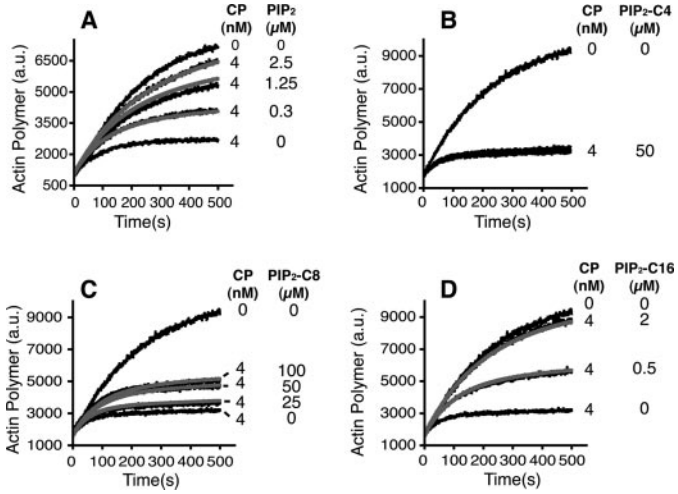

FIGURE 1. **Assay of PIP$_2$ acyl chain variants for the ability to inhibit the capping activity of CP.** In all experiments, 1.5 μM monomeric actin was present along with spectrin-actin seeds. Experimental data and fits are shown in *black* and *gray*, respectively. *A*, full-length PIP$_2$. Capping activity was completely inhibited with 5 μM PIP$_2$ (data not shown). *B*, PIP$_2$-diC$_4$. Capping activity is unaffected. *C*, PIP$_2$-diC$_8$. Partial inhibition of capping. *D*, PIP$_2$-diC$_{16}$. *a.u.*, arbitrary units.

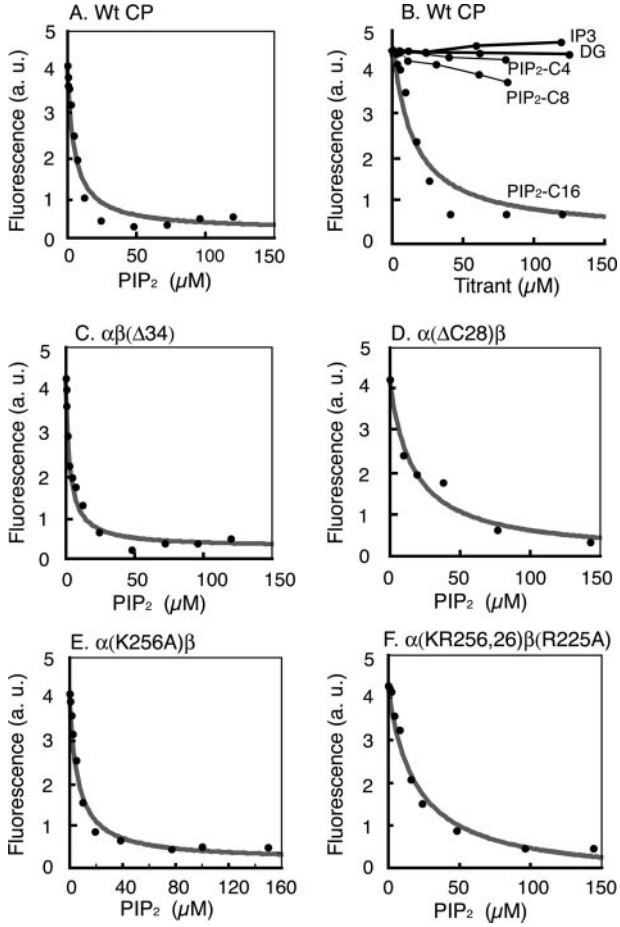

FIGURE 2. **PIP$_2$ interaction with CP by quenching of intrinsic tryptophan fluorescence.** Fluorescence intensity is plotted against the concentration of PIP$_2$ or other titrants. Experimental data and fits are shown in *black* and *gray*, respectively. *A*, wild-type (*Wt*) CP with natural PIP$_2$. *B*, wild-type CP with inositol trisphosphate (*IP$_3$*), diacylglycerol (*DG*), and synthetic PIP$_2$ variants. *C*, CP$\alpha\beta$(CΔ34) with PIP$_2$. *D*, CPα(CΔ28)β with PIP$_2$. *E*, CPα(K256A)β with PIP$_2$. *F*, CPα(R256A,K260A)β(R225A) with PIP$_2$. *a.u.*, arbitrary units.

the ability of PIP$_2$ and related compounds to inhibit CP in an actin polymerization capping assay and to quench the intrinsic tryptophan fluorescence of CP. In previous studies with micelles, the degree of phosphorylation of the inositol group was found to be important, as was the anionic character of the head group in general (28).

We reasoned that the micellar structure of PIP$_2$ in solution might be important for its ability to bind CP, because of the clustering of anionic head groups on the micelle surface. This hypothesis is supported by previous observations that dilution of PIP$_2$ with Triton X-100, which forms small micelles, abolishes the ability of PIP$_2$ to inhibit CP but that dilution with liposome-forming lipids does not (28). To test this idea further, we used synthetic versions of PIP$_2$ with shorter acyl chains. The diC$_4$, diC$_8$, and diC$_{16}$ synthetic forms of PIP$_2$ have 4, 8, and 16 carbons per acyl chain, respectively, whereas PIP$_2$ purified from natural sources has one C$_{18}$ and one C$_{20}$ chain. Purified PIP$_2$ at concentrations up to 5 μM completely inhibited the capping activity of 4 nM CP (Fig. 1*A*). The curves were fit well by a simple model of CP binding to PIP$_2$ (Fig. 1*A*, *gray lines*), with a K_d of 0.33 $\pm$ 0.04 μM. diC$_4$-PIP$_2$ showed no effect on the actin capping activity of CP (Fig. 1*B*), and diC$_8$-PIP$_2$ inhibited CP partially, with an apparent K_d of 68 μM (Fig. 1*C*). These concentrations are below the expected CMC (critical micellar concentration) values for diC$_4$- and diC$_8$-PIP$_2$ (29, 30). diC$_{16}$-PIP$_2$ inhibited CP completely with a K_d of $\sim$ 0.3 μM (Fig. 1*D*), comparable with the value for PIP$_2$, which is less than the expected CMC value.

To test physical binding, we used quenching of intrinsic tryptophan fluorescence (10). PIP$_2$ quenched the intrinsic tryptophan fluorescence of CP, with no change in the maximum emission wavelength. The effect was saturable at high PIP$_2$ concentration (Fig. 2*A*). A simple 1:1 binding model fit the data well (Fig. 2*A*, *gray lines*), with a K_d of 5.2 $\pm$ 0.2 μM, similar to a previous value for mouse CP in this type of assay (10). diC$_4$-PIP$_2$ and diC8-PIP$_2$ had little effect, whereas diC$_{16}$-PIP$_2$ produced saturable quenching with a K_d of 7 μM (Fig. 2*B*), close to the value for purified PIP$_2$. These result support the notion that the ability of PIP$_2$ to assemble in micelles is important for binding and inhibition of CP, presumably because of multimerization of the anionic head groups.

Next, we tested the head group alone, by using IP$_3$ (inositol-1,4,5 triphosphate). In an actin polymerization seeded growth assay, IP$_3$ at 100 μM had no effect on the capping activity of 4 nM CP (data not shown). In a tryptophan fluorescence titration, addition of IP$_3$ to concentrations $>$100 μM had no effect on the fluorescence of CP (Fig. 2*B*). As part of this experiment, we tested diacylglycerol, to represent the lipid portion of PIP$_2$. Again, no effect was seen (Fig. 2*B*). Thus, neither the head group nor the lipid backbone of the PIP$_2$ molecule is sufficient to bind CP, even at high concentrations.

Computational Docking Analysis of PIP$_2$/CP Interaction—To predict potential sites of interaction between PIP$_2$ and CP, we used a computational molecular docking approach. We began with a collection of CP structures produced by molecular dynamics simulation. The use of multiple structures for CP allowed us to sample different side chain and backbone conformations, and because we performed flexible docking where the

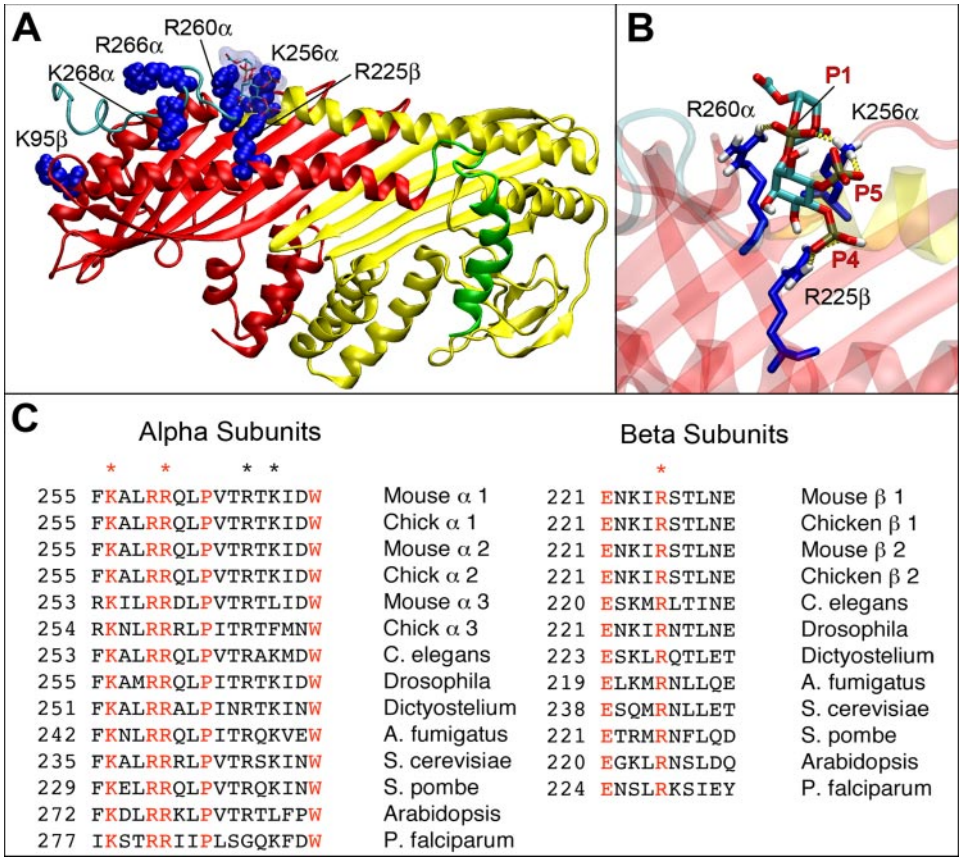

FIGURE 3. **Predictions for the binding site of PIP$_2$ on CP.** *A*, model of CP structure indicating the positions of the residues tested by mutagenesis. The α-monomer and α-tentacle are colored *yellow* and *cyan*, respectively, the β-monomer and β-tentacle are *red* and *green*, and PIP$_2$ is rendered in *stick* format with a *transparent blue* molecular surface. *B*, the molecular details of the interaction show binding to three basic groups on CP via electrostatic and hydrogen-bonding interactions (H-bonds are depicted as *dashed lines*). All molecular graphics were prepared using VMD (38). *C*, conservation of amino acid residues in the regions selected for mutagenesis in the α- and β-subunits of CP.

TABLE 1

Binding constants for the interaction of CP mutants with PIP$_2$ from tryptophan fluorescence quenching

The error values are standard deviations from multiple independent experiments or from the fitting procedure of single experiments.

CP species	K_d
	μM
α1β1	5.2 ± 0.2
α1β1	3.6 ± 0.6
α1β1(ΔC34)	3.1 ± 0.2
α1(ΔC28)β1	17
α1(K266AR68A)β1	5.1 ± 0.7
α1(K256A)β1	6.2 ± 0.7
α1(R260A)β1	3.6 ± 0.2
α1(R256AK60A)β1	12 ± 1.5
α1(K95A)β1	2.6 ± 0.5
α1β1(R225A)	2.8 ± 1.0
α1(R256A,K260A)β1(R225A)	19 ± 3

rotatable bonds in PIP$_2$ were allowed to move freely, this approach captured some degree of flexibility for both molecules. The molecular docking studies resulted in a clear single prediction for the structure of the complex of PIP$_2$ and CP. As one may have anticipated based on the anionic character of PIP$_2$, we saw interaction primarily with a group of basic residues on the surface of CP. This group included Lys-256 and Arg-260 of the α-subunit and Arg-225 of the β-subunit (Fig. 3, *A* and *B*). Given the residues and charged groups involved, the interactions are predominantly electrostatic in nature, with the addition of several hydrogen bonds (Fig. 3*B*). The inositol ring sits in a pocket formed by these residues, between the two subunits, and the location and orientation of these basic side chains suggests some degree of specificity for PI(4,5)P$_2$ *versus* other phosphoinositides, as observed previously (28).

In terms of the primary amino acid sequence, Lys-256 and Arg-260 are two residues in a conserved cluster of multiple basic residues near the C terminus of the CP α-subunit (Fig. 3*C*). Among these conserved basic residues, the CP crystal structure shows that Lys-256, Arg-260, Arg-266, and Lys-268 are on the surface and exposed to solvent (Fig. 3*A*). In contrast, Arg-259 is conserved but buried, where it forms an ionic bond with the conserved acidic residue Glu-221 of the β-subunit. Residue Arg-225 of CP β is also highly conserved in sequence alignments and exposed to solvent in the crystal structure. The C-terminal region of the α-subunit has been implicated in binding to actin (17), so the presence of a PIP$_2$ micelle at this site would be expected to provide an effective steric block to actin binding, as seen for villin, for example (31).

Mutation of the Conserved Basic Residues—To test for involvement of this basic patch in binding PIP$_2$, we introduced point and truncation mutations into the region. First, we tested binding with tryptophan quenching as shown in Fig. 2 and Table 1. For the residues implicated by the computational docking analysis, the single mutants CP α1(K256A)β1, CP α1(R260A)β1 and CP α1β1(R225A) bound PIP$_2$ normally. The double mutant CP α1(R256A,K260A) β1 bound more weakly, with a K_d of 12 μM, compared with 5 μM for wild-type CP. The triple mutant CP α1(R256A,K260A)β1(R225A) had a higher K_d of 19 μM.

The α-subunit double mutant KR266,268AA bound to PIP$_2$ with normal affinity (Table 1). Truncation of 28 residues from the C terminus of the α-subunit removes the final helix, including Arg-260, Lys-266, and Arg-268, and leaves Leu-258 as the C-terminal residue. This mutant is known to bind actin poorly (17). The affinity of the CP α Δ28 truncated protein for PIP$_2$ was decreased, with a K_d of 17 μM (Fig. 2, Table 1).

The C-terminal region of the β-subunit of CP also appears to function as a binding site for actin, independently of the α C terminus (17). Truncation of the β-subunit by 34 residues had no effect on the ability of CP to bind PIP$_2$ in the tryptophan quenching assay (Fig. 2, Table 1).

We next tested all of these CP mutants for interaction with PIP_2 based on inhibition of capping activity in actin polymerization assays. As part of this analysis, we first determined the affinity of the CP mutants for the F-actin barbed end, *i.e.*"K_{cap}." These values are required in order to calculate the binding constant for the CP/PIP_2 interaction. Wild-type CP ($\alpha1\beta1$) inhibited actin polymerization at barbed ends of actin filaments created by spectrin-actin seeds in a dose-dependent manner (Fig. 4*A*, *black lines*). Kinetic modeling gave good fits (Fig. 4*A*, *gray lines*), with a K_{cap} of 0.1 ± 0.05 nM (Table 2), similar to previous results (17). The α-subunit single and double mutations K256A,R260A, K266A,R268A, and R256A,K260A produced small to moderate increases in K_{cap}, with values of 0.18, 0.36, 0.4, and 1.3 nM, respectively (Fig. 4, Table 2). The β-subunit single mutant R225A also showed a moderate increase in K_{cap} to 1.2 nM. The triple mutant CPα(R256A,K260A)β(R225A) capped actin weakly (Fig. 4*F*), with a K_{cap} of 45 nM, which was mainly because of an increase in the off-rate constant (Table 2). The α-subunit truncation mutant CP$\alpha(\Delta28)\beta$ capped actin filaments weakly, with a K_{cap} of 1570 nM, and the β-subunit truncation mutant CP$\alpha\beta(\Delta34)$ capped actin with a K_{cap} of 10.5 nM (Table 2), consistent with previous studies (17).

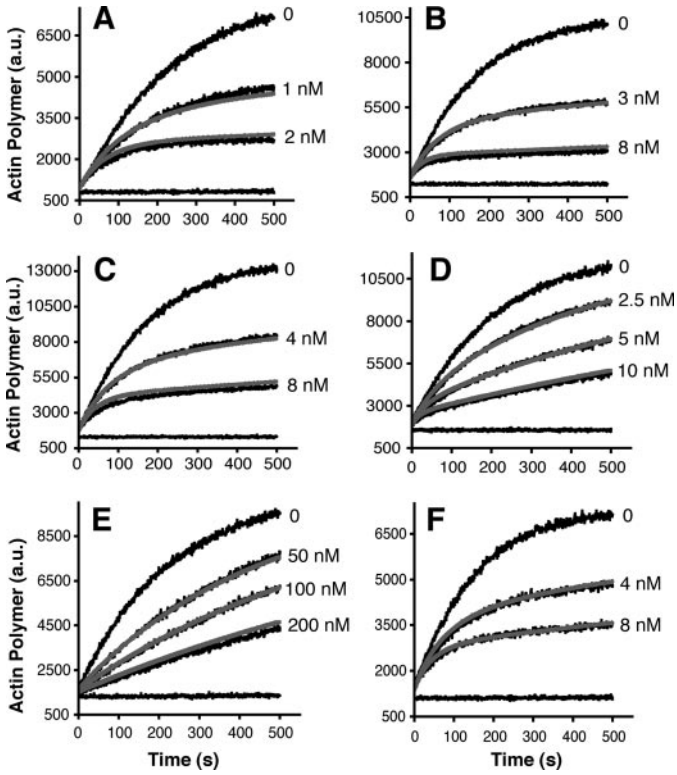

FIGURE 4. **Actin capping assays with CP and mutants.** CP concentrations were as indicated, with actin monomer and seeds as in Fig. 1. Experimental data and fits are shown in *black* and *gray*, respectively. *A*, wild-type CP$\alpha\beta$. *B*, CPα(K256A)β. *C*, CPα(R260A)β. *D*, CPα(R256A,K260A)β. *E*, CPα(R256A,K260A)β(R225A). *F*, CPα(K266A,R268A)β. *a.u.*, arbitrary units.

With values for K_{cap} in hand, we then repeated the assays with increasing concentrations of PIP_2 and used kinetic modeling to fit the curves and determine K_d values for the interaction of the CP mutants with PIP_2 (Fig. 5, Table 3). The α-subunit single and double mutations K256A, R260A, K266A,R268A, and R256A,K260A produced small to moderate increases in the K_d, with values of 0.31, 0.36, 0.41 and 3.9 μM, respectively (Table 3). The β-subunit single mutant R225A showed no increase in K_d. The triple mutant CP α(R256A,K260A)β(R225A) gave a ~60-fold increase in K_d to 21 μM (Fig. 5*F* and Table 3). For the α-subunit truncation mutant CP$\alpha(C\Delta28)\beta$, the K_d was 42 μM, ~130-fold greater than the value for wild-type CP (Fig. 5*A*, Table 3). The β-subunit truncation mutant CP$\alpha\beta(\Delta34)$ had a K_d of 1.6 μM (Fig. 5*B*, *gray lines*, and Table 3).

Nitrate Ions in the Crystal Structure—Nitrate ions can occupy phosphate-binding sites, and CP was crystallized in the presence of nitrate (14). The crystal structure has two nitrate ions in contact with the surface of the β-subunit. One interacts with Lys-95, and the other interacts with the helix dipole of helix 5. We mutated Lys-95 to alanine to make CP $\alpha\beta$(K95A). We found that this mutant capped actin with a normal affinity (Table 2), and its affinity for PIP_2 was the same as that of wild-type CP in both the actin capping and tryptophan fluorescence assays (Tables 1 and 3).

Direct Observation of Uncapping by PIP$_2$—One prediction of the wobble model is that an inhibitor of capping that does not bind to the CP β-subunit tentacle, about which the wobbling is proposed to occur, should be able to uncap. Indeed, previous studies showed that addition of PIP_2 to capped actin filaments in a polymerization reaction leads to an increase in the polymerization rate consistent with complete and rapid uncapping (11). Here, we tested uncapping with a more direct assay in which individual actin filaments are visualized by TIRF microscopy. In these experiments, movies reveal actin filaments growing from their ends. When CP was added, the growth stopped. Subsequent addition of PIP_2 caused the ends to return to the

TABLE 2

Binding constants for the interaction of CP with actin

K_{cap} was calculated from rate constants produced by fitting the time course of polymerization with Reaction 2 (see "Experimental Procedures"). Values are means ± S.E.

CP species	K_{cap}	k_{+cap}	k_{-cap}
	nM	$\mu M^{-1} s^{-1}$	s^{-1}
$\alpha1\beta1$	0.1 ± 0.05	5.74 ± 0.9	$5.7 \pm 2.2 \times 10^{-4}$
$\alpha1\beta1$	0.06 ± 0.02	8.8 ± 1.1	$6.4 \pm 1.5 \times 10^{-4}$
$\alpha1$(K256A)$\beta1$	0.18 ± 0.01	4.67 ± 0.04	$8.1 \pm 0.2 \times 10^{-4}$
$\alpha1$(R260A)$\beta1$	0.36 ± 0.04	3.1 ± 0.06	$1.1 \pm 0.1 \times 10^{-3}$
$\alpha1$(R256A,K260A)$\beta1$	1.3 ± 0.06	4.15 ± 0.27	$5.4 \pm 0.4 \times 10^{-3}$
$\alpha1\beta1$(K95A)	0.06 ± 0.02	9.5 ± 1	$6 \pm 2 \times 10^{-4}$
$\alpha1\beta1$(R225A)	1.2 ± 0.6	3.0 ± 1.1	$3.2 \pm 0.6 \times 10^{-3}$
$\alpha1$(K266A,R268A)$\beta1$	0.4 ± 0.1	2.6 ± 0.1	$1.1 \pm 0.3 \times 10^{-3}$
$\alpha1$(R256A,K260A)$\beta1$(R225A)	45 ± 4	1.01 ± 0.15	$4.5 \pm 0.3 \times 10^{-2}$
$\alpha1(\Delta C28)\beta1$	1570 ± 260	0.09 ± 0.014	0.14 ± 0.045
$\alpha1\beta1(\Delta C34)$	10.5 ± 1.7	1.1 ± 0.12	$1 \pm 0.2 \times 10^{-2}$

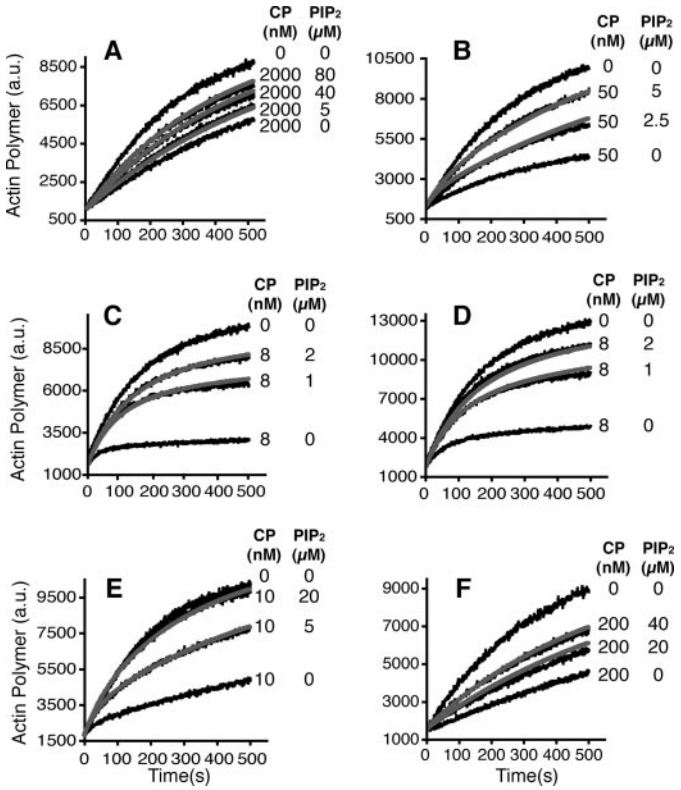

FIGURE 5. **PIP$_2$ binding affinities of CP mutants.** Concentrations of CP and PIP$_2$ were as indicated, with actin monomer and seeds as described in the legend for Fig. 1. Experimental data and fits are shown in *black* and *gray*, respectively. *A*, CPα(ΔC28)β. *B*, CP $\alpha\beta$(ΔC34). *C*, CPα(K256A)β. *D*, CPα(R260A)β. *E*, CPα(R256A,K260A)β. *F*, CPα(R256A,K260A)β(R225A). *a.u.*, arbitrary units.

TABLE 3

Binding constants for the interaction of CP with PIP$_2$ based on seeded actin polymerization assays

The K_d for CP binding to PIP$_2$ was calculated from the rate constants produced by fitting the time course of actin polymerization with Reaction 3 (see "Experimental Procedures").

CP species	K_d	k_+	k_-
	μM	$\mu M^{-1} s^{-1}$	s^{-1}
$\alpha1\beta1$	0.33 ± 0.04	2.0 ± 0.9	0.71 ± 0.4
$\alpha1\beta1$	0.25 ± 0.03	0.87 ± 0.13	0.21 ± 0.02
$\alpha1$(K256A)$\beta1$	0.31 ± 0.05	6.79 ± 0.72	2.08 ± 0.23
$\alpha1$(R260A)$\beta1$	0.36 ± 0.06	7 ± 2.6	2.6 ± 1.2
$\alpha1$(R256A,K260A)$\beta1$	3.9 ± 1.1	5.3 ± 1.5	19.6 ± 2.2
$\alpha1$(K266A,R268A)$\beta1$	0.41 ± 0.2	3.6 ± 0.4	1.5 ± 0.8
$\alpha1\beta1$(K95A)	0.27, 0.21	3.8, 1.0	1.0, 0.2
$\alpha1\beta1$(R225A)	0.22 ± 0.01	2.2 ± 1.2	0.48 ± 0.26
$\alpha1$(R256A,K260A)$\beta1$(R225A)	21.4 ± 0.4	1.65 ± 0.4	35.3 ± 8
$\alpha1$(ΔC28)$\beta1$	41.9 ± 12.3	6.7 ± 1.5	281 ± 31.5
$\alpha1\beta1$(ΔC34)	1.6 ± 0.3	0.97 ± 0.24	1.6 ± 0.5

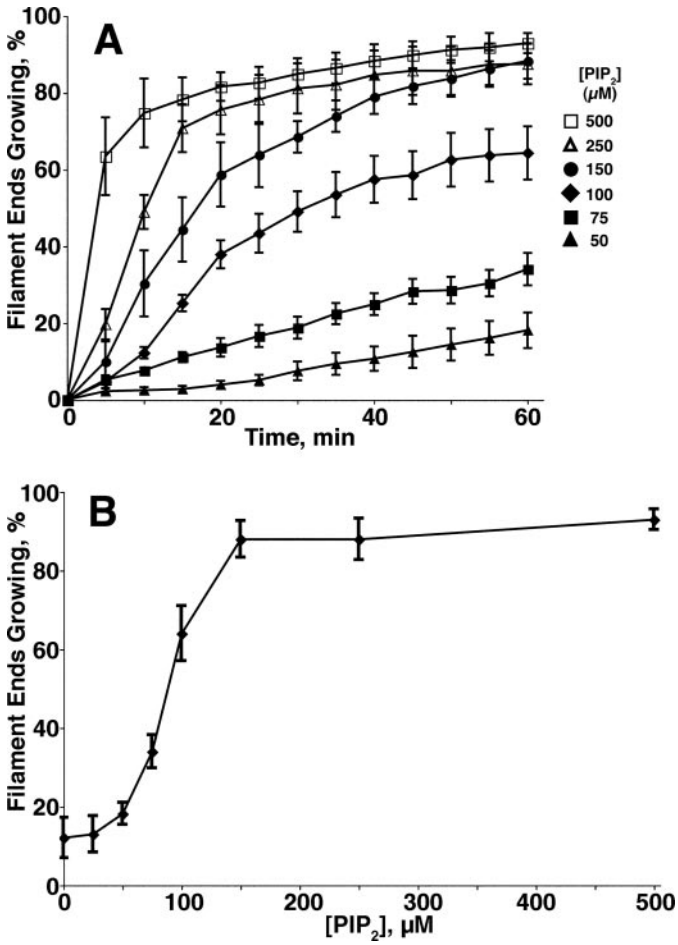

FIGURE 6. **Uncapping of capped actin filaments by PIP$_2$.** These data are derived from TIRF microscopy movies, one of which is in the supplemental materials. *A*, percentage of growing filaments is plotted *versus* time as a function of PIP$_2$ concentration. The results for 0, 25, and 50 μM PIP$_2$ largely overlapped, and therefore only one is shown. *B*, the percentage of growing filaments at 60 min is plotted *versus* PIP$_2$ concentration based on the data in *A*.

growing state (Fig. 6*A* and supplemental Movie 1). The mean rate of growth was 3.4 ± 0.3 subunits/s before capping and 2.8 ± 0.4 subunits/s after uncapping, in the presence of 2.0 μM monomeric actin. The effect of PIP$_2$ was nearly complete and relatively rapid, which is comparable with previous results with assays in solution (11). The fraction of ends converted from the capped to the growing state increased with PIP$_2$ concentration (Fig. 6*B*). The concentration of PIP$_2$ producing a half-maximal effect in this assay was ~100 μM, substantially higher than those seen with the tryptophan fluorescence and actin capping assays above. This may reflect sequestration of PIP$_2$ by the relatively large surface of bovine serum albumin-coated glass in this assay or perhaps a decreased accessibility of the actin filaments because of tethering at the surface.

DISCUSSION

In this study we performed a structure/function analysis to identify regions of CP necessary for interaction with PIP$_2$. The analysis was directed by predictions from computational modeling of CP/PIP$_2$ interactions, and the computational results were consistent with the functional and physical assays of the interaction. In addition, direct visualization of actin filament growth by TIRF microscopy provided new direct evidence of uncapping. Together, the results support the wobble model for the interaction of CP with the barbed end of the actin filament.

Nature of the Interaction between CP and PIP$_2$—We sought evidence of what regions of CP were needed for its interaction with PIP$_2$ by site-directed mutagenesis, changing single amino acids and truncating the C termini of the two subunits of the heterodimer. In previous studies, clusters of basic residues on the surface of proteins were implicated in binding PIP$_2$. For example, crystal structures of an AP180 protein complexed with phosphatidylinositols reveal a surface-exposed binding site composed of three lysine residues and one histidine, which

contact the phosphate groups (32). Sequence analysis of related proteins, combined with mutagenesis, identified a consensus binding sequence of KX_9KX(K/R)(H/Y). PIP$_2$ binds and inhibits a number of actin-binding proteins, including profilin and the gelsolin family, and a number of studies identify (K/R)X_{3-5}(K/R)X(K/R)(K/R) as a consensus binding site (31, 33, 34).

In addition, we know that CP from every organism tested, including yeast, plants and mammals, is inhibited by PIP$_2$ (10). Therefore, we focused on conserved clusters of basic residues on the surface of the protein. The largest and most distinct cluster is in and around the C-terminal region of the α-subunit, including its connection to the body of the protein. A recent study of phosphoinositides interacting with *Arabidopsis* CP also noted the existence of this conserved basic region and suggested that it might be important (10). Indeed, we found that a cluster of three conserved basic residues on the surface, near the α C terminus, were important for binding PIP$_2$. These include Lys-256 and Arg-260 of the α-subunit and Arg-225 of the β-subunit. In contrast, two nearby basic residues, also conserved and on the surface, were not important.

Computational docking studies provide complementary evidence for the primary role of these three residues. Of note, the docking studies were done largely in advance of the mutagenesis studies, and they helped us to narrow and define our list of potential mutants. A recent computational study of CP interacting with lipids, including ones other than polyphosphoinositides, raises the possibility that portions of CP may become partially buried in the lipid bilayer (35). One of several regions identified as potentially important in that study was the 215–232 region of the β-subunit, which includes Arg-225, one of the three residues identified as important in our results here. The notion of lipid binding to the interior of CP may be supported by an early study in which, by gel filtration analysis, micelles of PIP$_2$ appeared to partially dissociate the α- and β-subunits (28).

Implications for How CP Binds Actin—As part of our analysis, we tested the ability of a number of new point mutants of CP to cap actin filaments. Previous studies, largely with truncations, had implicated the C-terminal region of the α-subunit as important, and these new point mutations help to define the residues important for binding actin more closely. Of note, a cluster of three conserved basic residues on the surface, near the α C terminus, were found to be important, including Lys-256 and Arg-260 of the α-subunit and Arg-225 of the β-subunit. Two other basic conserved surface residues located nearby, Arg-266 and Lys-268 of the α-subunit, were found to be much less important. These results do not show that these residues bind actin directly. This will require further studies, including structural ones. A recent cryo-electron microscopy study indicates that Arg-260, Arg-266, and Lys-268 are among a cluster of basic of residues making close contact with nearby Lys-256 (15).

Implications for the Wobble Hypothesis—As originally suggested by the analysis of the crystal structure of CP (14), we currently hypothesize that CP has two independent sites for binding to the barbed end of the actin filament. One includes the C-terminal "tentacle" of the β-subunit, so-named because it is surrounded by solvent in the crystal structure and is highly mobile in molecular dynamics simulations (6, 14). The other involves the C-terminal region of the α-subunit. However, in this case, the region does not appear to be mobile, based on S100 inhibitor and molecular dynamics studies (6, 14). CP bound to the barbed end of the actin filament appears to utilize both sites (17). We hypothesize that they can dissociate independently, which predicts that CP bound only by its β-tentacle should be relatively mobile and "wobble" on the barbed end of the filament. One prediction of the model is that a molecule that binds to CP at the second actin-binding site, near the α C terminus, should be able to bind to the wobble state and thereby promote dissociation and thus "uncapping."

Our results here with PIP$_2$ confirm this prediction. First, the point mutations near the α C terminus show that this region is involved in binding actin and PIP$_2$. Second, PIP$_2$ can induce uncapping, as visualized here in real time with TIRF microscopy of polymerizing actin filaments. A complementary prediction and confirmation of the model was provided by our recent results with V-1/myotrophin, which binds to CP and inhibits actin binding but does so by interacting with the β-tentacle (6). In this case, the model predicts that uncapping will not occur, and that was the result.

Implications for Actin Assembly in Cells—CP is an essential element of the dendritic nucleation model, and consistent with that view, loss of CP leads to loss of lamellipodia in cultured cells (3). In this model, barbed ends are created near the plasma membrane and grow for a time before being capped by CP. One simple hypothesis based on our results is that PIP$_2$ in the plasma membrane, acting as a second messenger, will inhibit capping and thus promote actin polymerization at the membrane. Indeed, overexpression of phosphatidylinositol 5-kinase can lead to rocketing of membrane vesicles in the cell (36, 37).

A more interesting and speculative hypothesis is that PIP$_2$ or other molecules that can cause uncapping, such as the protein CARMIL (9), might be responsible for promoting disassembly of actin filaments in zones of depolymerization or for providing a source of free barbed ends. The latter has been suggested by studies of platelet activation, where explosive actin polymerization occurs (12).

REFERENCES

1. Wear, M. A., and Cooper, J. A. (2004) *Trends Biochem. Sci.* **8,** 418–428
2. Pollard, T. D., and Borisy, G. G. (2003) *Cell* **4,** 453–465
3. Mejillano, M. R., Kojima, S., Applewhite, D. A., Gertler, F. B., Svitkina, T. M., and Borisy, G. G. (2004) *Cell* **3,** 363–373
4. Loisel, T. P., Boujemaa, R., Pantaloni, D., and Carlier, M. F. (1999) *Nature* **6753,** 613–616
5. Kim, K., Galletta, B. J., Schmidt, K. O., Chang, F. S., Blumer, K. J., and Cooper, J. A. (2006) *Mol. Biol. Cell* **17,** 1354–1363
6. Bhattacharya, N., Ghosh, S., Sept, D., and Cooper, J. A. (2006) *J. Biol. Chem.* **281,** 31021–31030
7. Bruck, S., Huber, T. B., Ingham, R. J., Kim, K., Niederstrasser, H., Allen, P. M., Pawson, T., Cooper, J. A., and Shaw, A. S. (2006) *J. Biol. Chem.* **281,** 19196–19203
8. Canton, D. A., Olsten, M. E., Niederstrasser, H., Cooper, J. A., and Litchfield, D. W. (2006) *J. Biol. Chem.* **281,** 36347–36359
9. Yang, C., Pring, M., Wear, M. A., Huang, M., Cooper, J. A., Svitkina, T. M., and Zigmond, S. H. (2005) *Dev. Cell* **2,** 209–221
10. Huang, S., Gao, L., Blanchoin, L., and Staiger, C. J. (2006) *Mol. Biol. Cell* **17,** 1946–1958
11. Schafer, D. A., Jennings, P. B., and Cooper, J. A. (1996) *J. Cell Biol.* **1,** 169–179

12. Barkalow, K., Witke, W., Kwiatkowski, D. J., and Hartwig, J. H. (1996) *J. Cell Biol.* **2,** 389–399
13. Eddy, R. J., Han, J., and Condeelis, J. S. (1997) *J. Cell Biol.* **139,** 1243–1253
14. Yamashita, A., Maéda, K., and Maéda, Y. (2003) *EMBO J.* **7,** 1529–1538
15. Narita, A., Takeda, S., Yamashita, A., and Maeda, Y. (2006) *EMBO J.* **25,** 5626–5633
16. Kim, K., Yamashita, A., Wear, M. A., Maeda, Y., and Cooper, J. A. (2004) *J. Cell Biol.* **4,** 567–580
17. Wear, M. A., Yamashita, A., Kim, K., Maéda, Y., and Cooper, J. A. (2003) *Curr. Biol.* **13,** 1531–1537
18. Soeno, Y., Abe, H., Kimura, S., Maruyama, K., and Obinata, T. (1998) *J Muscle Res. Cell Motil.* **6,** 639–646
19. DiNubile, M. J., Cassimeris, L., Joyce, M., and Zigmond, S. H. (1995) *Mol. Biol. Cell* **12,** 1659–1671
20. Pollard, T. D. (1986) *J. Cell Biol.* **103,** 2747–2754
21. Wear, M. A., and Cooper, J. A. (2004) *J. Biol. Chem.* **279,** 14382–14390
22. Kuhn, J. R., and Pollard, T. D. (2005) *Biophys. J.* **88,** 1387–1402
23. Kron, S. J., and Spudich, J. A. (1986) *Proc. Natl. Acad. Sci. U. S. A.* **83,** 6272–6276
24. Huxley, H. E., and Brown, W. (1967) *J. Mol. Biol.* **30,** 383–434
25. Kale, L., Skeel, R., Bhandarkar, M., Brunner, R., Gursoy, A., Krawetz, N., Phillips, J., Shinozaki, A., Varadarajan, K., and Schulten, K. (1999) *J. Comput. Phys.* **151,** 283–312
26. Mitra, A., and Sept, D. (2004) *Biochemistry* **43,** 13955–13962
27. Morris, G. M., Goodsell, D. S., Halliday, R. S., Huey, R., Hart, W. E., Belew, R. K., and Olson, A. J. (1998) *J. Comput. Chem.* **19,** 1639–1662
28. Heiss, S. G., and Cooper, J. A. (1991) *Biochemistry* **30,** 8753–8758
29. Campbell, R. B., Liu, F., and Ross, A. H. (2003) *J. Biol. Chem.* **278,** 33617–33620
30. Rebecchi, M. J., Eberhardt, R., Delaney, T., Ali, S., and Bittman, R. (1993) *J. Biol. Chem.* **268,** 1735–1741
31. Kumar, N., Zhao, P., Tomar, A., Galea, C. A., and Khurana, S. (2004) *J. Biol. Chem.* **279,** 3096–3110
32. Ford, M. G., Pearse, B. M., Higgins, M. K., Vallis, Y., Owen, D. J., Gibson, A., Hopkins, C. R., Evans, P. R., and McMahon, H. T. (2001) *Science* **291,** 1051–1105
33. Yu, F.-X., Sun, H.-Q., Janmey, P. A., and Yin, H. L. (1992) *J. Biol. Chem.* **267,** 14616–14621
34. Janmey, P. A., Xian, W., and Flanagan, L. A. (1999) *Chem. Phys. Lipids* **101,** 93–107
35. Smith, J., Diez, G., Klemm, A. H., Schewkunow, V., and Goldmann, W. H. (2006) *Theor. Biol. Med. Model.* **3,** 30
36. Rozelle, A. L., Machesky, L. M., Yamamoto, M., Driessens, M. H., Insall, R. H., Roth, M. G., Luby-Phelps, K., Marriott, G., Hall, A., and Yin, H. L. (2000) *Curr. Biol.* **6,** 311–320
37. Schafer, D. A., Welch, M. D., Machesky, L. M., Bridgman, P. C., Meyer, S. M., and Cooper, J. A. (1998) *J. Cell Biol.* **7,** 1919–1930
38. Humphrey, W., Dalke, A., and Schulten, K. (1996) *J. Mol. Graph.* ***14,*** *33-* **8,** 27–28